Journal of Southeast University (English Edition) Vol. 35, No. 1, pp. 83 - 88 Mar. 2019 ISSN 1003—7985

Effect of flexural loading on degradation progress of recycled aggregate concrete subjected to sulfate attack and wetting-drying cycles

Zhao Yasong Gao Jianming Qi Bing Liu Chuanbei

(School of Materials Science and Engineering, Southeast University, Nanjing 211189, China)
(Jiangsu Key Laboratory of Construction Materials, Southeast University, Nanjing 211189, China)

Abstract: The degradation progress of recycled aggregate concrete (RAC) subjected to sulfate attack under wetting-drying cycles and flexural loading is studied. Three different stress ratios (0, 0.3 and 0.5) were applied in this test. The variations of relative dynamic elastic modulus E_{rd} and water-soluble SO_4^{2-} contents in RAC were used to evaluate degradation progress. The changes in mineral products and microstructures of interior concrete were investigated by means of X-ray diffraction (XRD), the environmental scanning electron microscope (ESEM) and X-ray computed tomography (X-CT). The results indicate that flexural loading accelerates the degradation of RAC under sulfate attack and wetting-drying cycles by expediting the transmission of SO_4^{2-} into interior concrete. Furthermore, the accelerated effect of flexural loading is more obvious with the increase of stress ratio, that is because higher stress ratios can accelerate the extension of microcracks and generate more channels for the transmission of SO_4^{2-}. Also, more expansive products (gypsum and ettringite) are generated by the reaction of $Ca(OH)_2$ with SO_4^{2-}, which can further accelerate the degradation of RAC.

Key words: recycled aggregate concrete; degradation; sulfate attack; flexural loading; wetting-drying cycles
DOI: 10.3969/j.issn.1003-7985.2019.01.012

Over the past decades, vast amounts of construction and demolition wastes (C&DW) have been generated due to the urbanization in China, and waste concrete has accounted for a large proportion of C&DW. It was reported that 100 million tons of waste concrete were generated every year, and occupied about 1/3 of total C&DW[1]. Therefore, the disposal of waste concrete has been an extremely urgent problem currently.

Received 2018-08-03, **Revised** 2019-01-04.

Biographies: Zhao Yasong (1993—), male, Ph.D. candidate; Gao Jianming (corresponding author), male, doctor, professor, 101000879@seu.edu.cn.

Foundation items: The National Natural Science Foundation of China (No. 51578141), the Major State Basic Research Development Program of China (No. 2015CB655102), China-Japanese Research Cooperative Program—Ministry of Science and Technology in China (No. 2016YFE0118200).

Citation: Zhao Yasong, Gao Jianming, Qi Bing, et. al. Effect of flexural loading on degradation progress of recycled aggregate concrete subjected to sulfate attack and wetting-drying cycles[J]. Journal of Southeast University (English Edition), 2019, 35(1): 83 - 88. DOI: 10.3969/j.issn.1003-7985.2019.01.012.

Some studies on properties of recycled concrete aggregate (RCA) have been carried out. Compared with natural aggregate, RCA from waste concrete has the properties of higher porosity, lower strength and more complicated microstructure on the surface. However, those RCA still can be used to prepare RAC[2-4]. Furthermore, some studies on high-performance concrete made with RCA also have been published[5-7]. The mechanical properties of RAC have been investigated for many years, and results indicate that adding RCA in concrete can result in the deterioration of mechanical properties[8-13]. Some research on durability of RAC has been carried out[14-16], but there is very little study on the degradation of RAC subjected to sulfate attack[17-18]. Especially in practical engineering, the RAC structure not only suffers from sulfate attack, but also will be subjected to flexural loading, which will largely affect the degradation progress of RAC under sulfate attack. Meanwhile, the status of RAC is not always be water-saturated, the wet and dry status will occur alternately. Therefore, it is necessary to investigate the effect of flexural loading on the degradation progress of RAC subjected to sulfate attack and wetting-drying cycles.

The purpose of this work is to evaluate the effect of flexural loading on the degradation process of RAC subjected to sulfate attack and wetting-drying cycles. Three different stress ratios (0, 0.3 and 0.5) were applied in this test, and RAC were exposed to a sodium sulfate solution (50 g/L) and wetting-drying cycles. The whole test lasted for 9 months, and during this period, samples were taken out to measure relative dynamic elastic modulus E_{rd} and water-soluble SO_4^{2-} contents. Meanwhile, the methods of XRD, ESEM and X-CT were used to analyze changes in mineral products and micro-structures of interior concrete.

1 Experimental Program

1.1 Materials and mix proportions

42.5R (Ⅱ) Portland cement was used in this study, complying with GB 175—2007. The chemical compositions of cement are shown in Tab. 1. RCA was from a demolition site in Nanjing with the maximum size of 20 mm. The properties of RCA are shown in Tab. 2, and Tab. 3 shows the mix proportion of RAC.

Tab. 1 Chemical compositions of cement %

$w(SiO_2)$	$w(Al_2O_3)$	$w(CaO)$	$w(MgO)$	$w(SO_3)$	$w(Fe_2O_3)$	Loss
21.20	5.32	64.37	0.55	2.00	4.42	1.50

Tab. 2 Physical properties of RCA

Apparent density/ ($kg \cdot m^{-3}$)	Water adsorption/ %	Crushing index value/ %
2 580	3.6	15.5

Tab. 3 Mix proportion of RAC kg/m^3

Water	Cement	Sand	RCA	Super plasticizer
195	390	740	1 024	0.49

1.2 Test setup and instrumentation

In this study, 51 RAC specimens with the size of 70 mm × 70 mm × 280 mm were prepared and six of them were used to test ultimate flexural strength, the others were separated into three groups to determine E_{rd} and the SO_4^{2-} content of RAC with different stress ratios. All specimens were demolded after 24 h of casing and then cured in standard curing ($T = (20 \pm 2)$ ℃, RH≥95%). After 60 d curing, specimens were covered with epoxy resin except for two opposite profiles (70 mm × 280 mm) to obtain the one-dimensional SO_4^{2-} transmission.

The four-point bending load device as shown in Fig. 1 was used to apply flexural loading. According to Hooke's law, the deformation of the spring can generate load to the steel plate, and this load will be transferred onto the specimens to form the four-point bending effect. Meanwhile, the relationship between the spring deformation and the value of generated load was determined. Hence, three stress ratios (0, 0.3 0.5) corresponding to 0, 30% and 50% of the ultimate flexural load were conducted to RAC and remained in the whole exposure period.

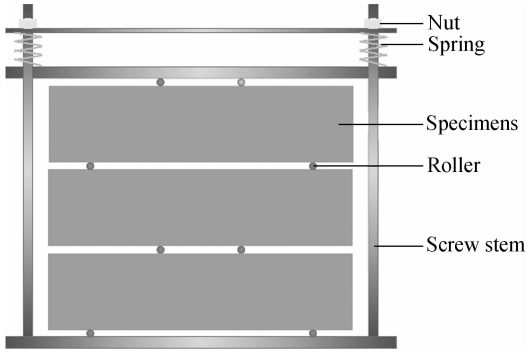

Fig. 1 Equipment for applying flexural loading

Sodium sulfate solution with the content of 50 g/L was used in this study to simulate the sulfate attack environment. As for wetting-drying regime, all specimens with applying flexural loading devices were immersed in a sodium sulfate solution for 21 h first, then followed by air-drying for 3 h. After that, they were dried for 45 h at a temperature of 60 ℃, then followed by air cooling for 3 h. The whole period of 72 h was regarded as a wetting-drying cycle.

The relative dynamic modulus of elasticity of the specimen, E_{rd}, was measured by a nonmetal ultrasonic analyzer (NM-4A, transducer frequency is 50 KHz). The surface of specimens will be uneven as a result of the erosion process; therefore, vaseline was used as a coupling agent to ensure the accuracy of measured values. The test length of specimens is 280 mm. The dynamic modulus elasticity of specimens E_d was determined by Eq. (1) before the wetting-drying cycles. Then, the changes of E_d were monitored after every 3 times of wetting-drying cycles. E_{rd} can be calculated by

$$E_d = \frac{(1+v)(1-2v)\rho V^2}{1-v} = \frac{(1+v)(1-2v)\rho L^2}{(1-v)t^2} \quad (1)$$

$$E_{rd} = \frac{E_{dn}}{E_{d0}} = \frac{V_n^2}{V_0^2} = \frac{t_0^2}{t_n^2} \quad (2)$$

where E_d is the dynamic modulus of elasticity of the specimen; E_{rd} is the relative dynamic modulus of elasticity of the specimen; V is the ultrasonic velocity, m/s; ρ is the density of the specimen, kg/m^3; v is the Poisson ratio; t is the sound interval, μs; L is the test distance of the specimen, m; t_0 is the sound-interval for the specimen before erosion, μs; t_n is the sound-interval for the specimen during the erosion test, μs.

The method of ultra-violet and visible spectrophotometer (UVPC) was used to determine the SO_4^{2-} content. The dried RAC sample was taken out from the bending load device, and then was drilled from the sulfate transfer side by the bench drilling machine. The sample powders from the depths of 0 to 5, 5 to 10, 10 to 15, 15 to 20 mm were collected. Then, the powder was dried until constant weight at 60 ℃. After that, 2 g powder was taken out to dissolve into 50 mL deionized water and stored for 24 h, then the mixture was filtered, and 25 mL solution was extracted into colorimetric cylinder. 2.5 mL hydrochloric acid (2.5 mL/L) and 10 mL $BaCl^{2-}$ PVA mixed solution were added into the colorimetric cylinder in turn. Then, 25 mL deionized water was added into the colorimetric cylinder and the solution was blended fully. Finally, the solution was moved into cuvette and tested. The SO_4^{2-} content of the sample can be calculated by taking absorbance of the prepared solution into Eq. (3).

First, the standard SO_4^{2-} solution was prepared by adding certain anhydrous sodium sulfate into deionized water, and then the standard curve of SO_4^{2-} content with absorbance of ultra-violet was determined and shown in Fig. 2. A nonlinear model of SO_4^{2-} content with absorbance of ultra-violet is

$$f(A) = 8.715\ 26A^2 + 3.383\ 241A - 0.256\ 43R^2 = 0.971\ 29 \quad (3)$$

2 Results and Discussion

2.1 Variations of E_{rd} for RAC

The variations of E_{rd} with time for RAC under different

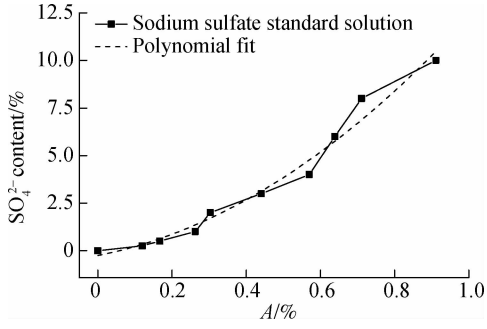

Fig. 2 Standard curve of sodium sulfate solution

stress ratios are shown in Fig. 3. It can be seen that the curves of E_{rd} for different stress ratios are similar, which are also quite similar to the curve of E_{rd} for ordinary concrete under sulfate attack. Three degradation stages under sulfate attack and wetting-drying cycles can be observed[18-19]. The first stage is called the initial damage stage as a result of wetting-drying cycles; this stage can last about 30 d and E_{rd} decreases to about 0.9. The reason is that when the RAC was taken out from the sulfate solution and dried in oven (60 ℃), the sulfate ions in concrete will gradually reach the supersaturation and generate the crystallization, which will lead to the internal stress and microcracks generated in the concrete[20-21]. The second stage is a linear increasing stage and E_{rd} increases in this stage. This phenomenon can be attributed to the generation of expansive products when SO_4^{2-} penetrates into RAC and reacts with internal hydration products, which can fill in the pores and interfacial transition zones (ITZ) to make the microstructure denser, so E_{rd} can increase over the time. However, when the expansion stress generated by expansive products exceeds the tensile strength of RAC, micro cracks will be generated and cause the accelerated penetration of SO_4^{2-}, so a vicious circle is created and the decreasing stage will appear.

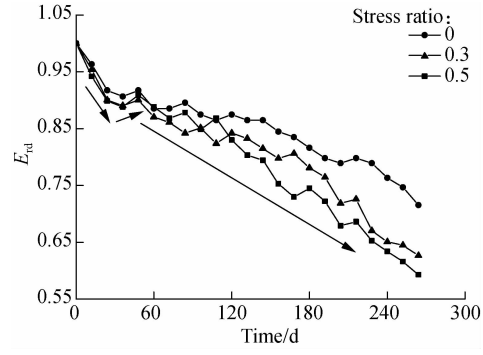

Fig. 3 E_{rd} variations for RAC under different stress ratios

Fig. 3 shows that the application of flexural loading can increase the deterioration of specimens under sulfate attack and wetting-drying cycles. After 270 d, the E_{rd} values of specimens with stress ratios 0.5 and 0.3 are 0.593 and 0.626, respectively, which are 17.1% and 12.5% lower than those of the specimens without loading, respectively. The reason can be that microcracks are more easily generated when the flexural loading is higher, so the expansive products can penetrate into concrete more quickly and result in acceleration of degradation progress.

2.2 SO_4^{2-} diffusion in concrete

Fig. 4 shows the water-soluble SO_4^{2-} content of specimens under different stress ratios calculated by Eq. (1) on different degradation days. It can be observed that the higher the stress ratio, the higher the water-soluble SO_4^{2-} content with the same attacking time and depth. For example, after a 30 d sulfate attack, the water-soluble SO_4^{2-} content with stress ratios 0.3 and 0.5 is 0.58% and 0.67% at the depth of 0 to 5 mm, respectively, which increases by 9.4% and 26.5% compared with that of the

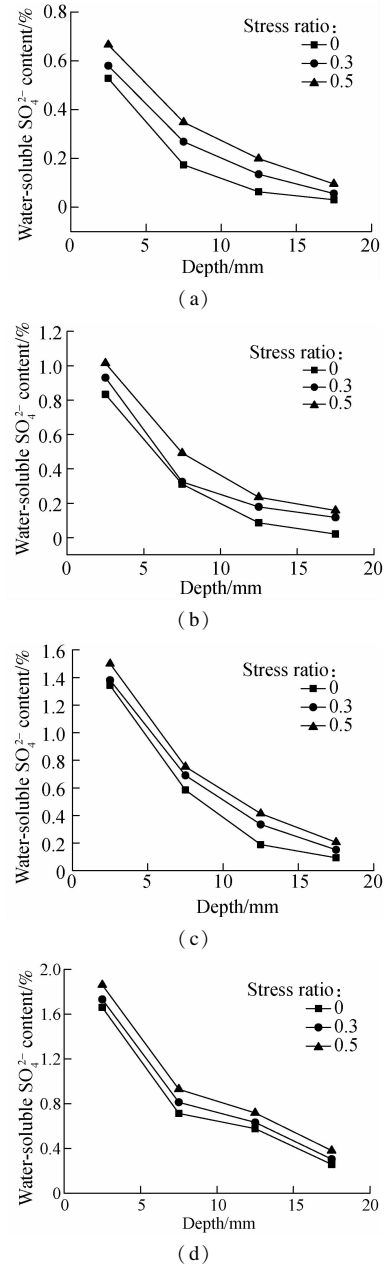

Fig. 4 Water-soluble SO_4^{2-} content for RAC under different stress ratios on different immersion days. (a) 30 d; (b) 90 d; (c) 180 d; (d) 270 d

specimen without loading, respectively. The reason is that the application of flexural loading can generate microcracks in concrete. Meanwhile, the sustained loading will accelerate the expansion of microcracks, and thus more channels for transmission of SO_4^{2-} are generated. The increase of stress ratio can cause more microcracks to be generated and then accelerate the transmission of SO_4^{2-}. This result is in accordance with the E_{rd} variation of RAC.

Meanwhile, the water-soluble SO_4^{2-} content at the same depth becomes greater with the increase of immersion time. For example, when the stress ratio is 0.5, the water-soluble SO_4^{2-} content at the depth of 0 to 5 mm is 0.67% after 30 d immersion. After 270 d immersion, the water-soluble SO_4^{2-} content is 1.86% at the same depth, which is attributed to the surface degradation and crack propagation of RAC under a sulfate attack.

2.3 XRD analysis

The reaction products of specimens were identified by the method of XRD. Fig. 5 shows the XRD patterns of RAC under different stress ratios after 270 d immersion. It can be clearly found that the main phases of specimens have no change. However, compared with a no-loading specimen, specimens with stress ratios 0.3 and 0.5 have a higher peak intensity of ettringite and gypsum and a lower peak intensity of $Ca(OH)_2$. It is revealed that the application of flexural loading can obviously accelerate the damage to the microstructure and provide more available spaces for expansive products (gypsum and ettringite) generated by the reaction of $Ca(OH)_2$ with SO_4^{2-}. Thus, the formation of expansive products will accelerate the degradation of RAC and cause E_{rd} reduction under a sulfate attack and wetting-drying cycles. The same chemical products have also been found in ordinary concrete under a sulfate attack and wetting-drying cycles[18, 20].

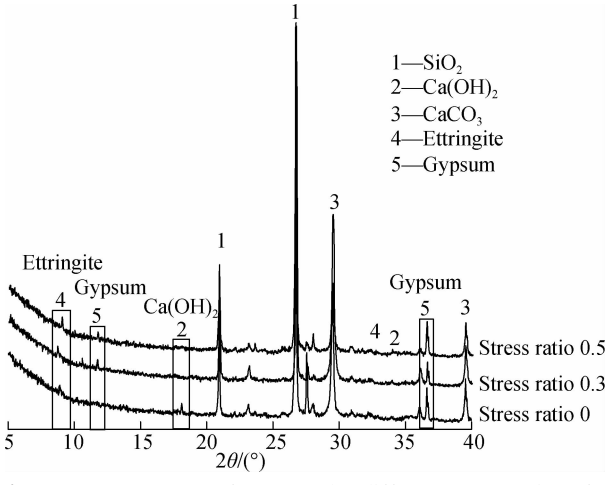

Fig. 5 XRD patterns of RAC under different stress ratios after 270 d immersion

2.4 Environmental scanning electron microscope (ESEM)

The variations of the microstructure of RAC under different stress ratios after 270 d immersion were observed by ESEM. It is clear that some needle-like corrosion products (ettringite) and short rod-like corrosion products (gypsum) can be observed in Fig. 6. Compared with the no-loading specimen, the amount of corrosion products in specimens with stress ratios 0.3 and 0.5 is much higher, and the short rod-like gypsum is the main corrosion product. The main reason is that SO_4^{2-} in RAC increases under the influence of flexural loading, and those SO_4^{2-} will react with C_3A and its hydration products first. After that, the gypsum will be generated by the reaction of $Ca(OH)_2$ with SO_4^{2-}. Therefore, the results of ESEM can provide a microscopic evidence for the phenomena in Sections 2.1 and 2.2.

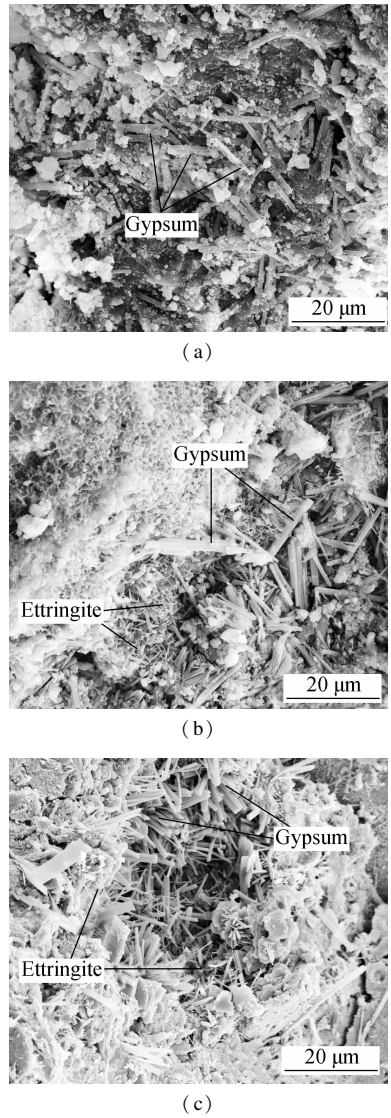

Fig. 6 ESEM images of RAC under different stress ratios after 270 d immersion. (a) Stress ratio is 0; (b) Stress ratio is 0.3; (c) Stress ratio is 0.5

2.5 X-ray computed tomography (X-CT)

X-CT was used to analyze the distribution of pores and cracks of RAC. After 270 d sulfate attack, the middle part of the experimental specimen (70 mm × 70 mm ×

70 mm) was cut out to be used as X-CT samples. The 3D stereograms and 2D slice diagrams of RAC under different stress ratios are shown in Fig. 7. The specimen in Figs. 7 (a) and (b) is RAC without flexural loading. It can be observed that the damage of RAC under sulfate attack and wetting-drying cycles is concentrated on the surface of the specimen, and a small number of cracks can be found in the interior of RAC. The cracks of RAC without loading are mainly caused by the salt crystallization and the formation of expansive corrosion products. Figs. 7 (c) to (f) reveal that the number of cracks of RAC rises obviously with the increase of stress ratio. In particular, more cracks are found inside the specimen when the stress ratio is 0.5. Therefore, when the flexural loading is applied on RAC, the degradation of RAC is not only caused by the salt crystallization and the formation of expansive corrosion products, the flexural loading can also accelerate the expansion of microcracks generated by corrosion, and this effect will be more pronounced with the increase of corrosion time. Hence, flexural loading can accelerate the degradation progress of RAC under a sulfate attack and wetting-drying cycles.

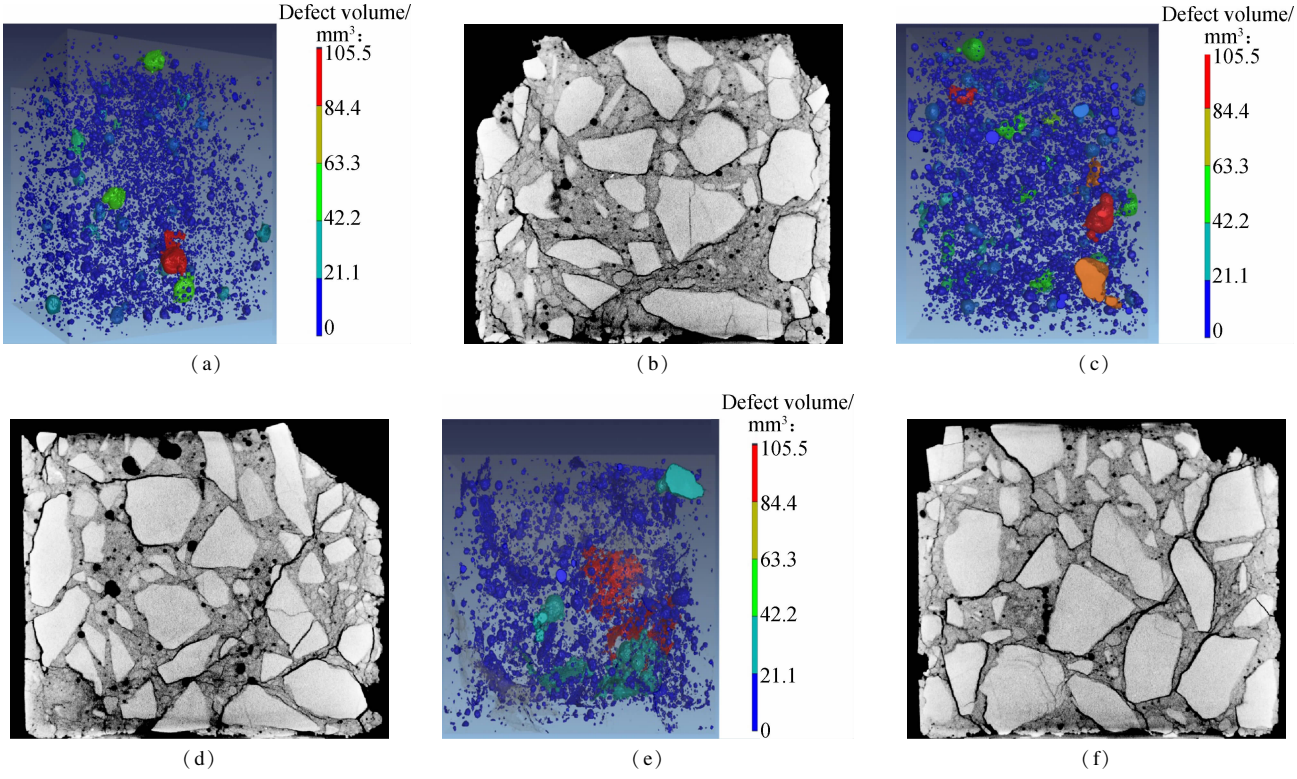

Fig. 7 X-CT images of RAC under different stress ratios after 270 d immersion. (a) 3D stereogram without stress ratio; (b) 2D slice diagram without stress ratio; (c) 3D stereogram under stress ratio 0.3; (d) 2D slice diagram under stress ratio 0.3; (e) 3D stereogram under stress ratio 0.5; (f) 2D slice diagram under stress ratio 0.5

3 Conclusions

1) The degradation progress of RAC under sulfate attack and wetting-drying cycles can be divided into three stages: The initial damage stage caused by wetting-drying cycles, the increasing and accelerated decreasing stages caused by expansive products generated by sulfate attack.

2) Flexural loading can accelerate the degradation progress of RAC. The expansion of microcracks will be accelerated as a result of applying flexural loading, and thus more channels for the transmission of SO_4^{2-} are generated inside the RAC and more corrosion products are produced.

3) The main corrosion products of RAC subjected to sulfate attack under drying-wetting cycles and flexural loading are gypsum and ettringite. The flexural loading can accelerate the generation of corrosion products.

References

[1] Xiao J Z. *Recycled concrete*[M]. Beijing: Chinese Building Construction Publishing Press, 2008: 85 – 88. (in Chinese)

[2] Silva R V, de Brito J, Dhir R K. Properties and composition of recycled aggregates from construction and demolition waste suitable for concrete production[J]. *Construction and Building Materials*, 2014, **65**: 201 – 217. DOI: 10.1016/j.conbuildmat.2014.04.117.

[3] de Juan M S, Gutiérrez P A. Study on the influence of attached mortar content on the properties of recycled concrete aggregate[J]. *Construction and Building Materials*, 2009, **23**(2): 872 – 877. DOI: 10.1016/j.conbuildmat.2008.04.012.

[4] Etxeberria M, Vázquez E, Marí A, et al. Influence of amount of recycled coarse aggregates and production process on properties of recycled aggregate concrete[J]. *Cement and Concrete Research*, 2007, **37**(5): 735 –

742. DOI:10.1016/j.cemconres.2007.02.002.
[5] Andreu G, Miren E. Experimental analysis of properties of high performance recycled aggregate concrete [J]. *Construction and Building Materials*, 2014, **52**: 227 - 235. DOI:10.1016/j.conbuildmat.2013.11.054.
[6] Kou S C, Poon C S. Effect of the quality of parent concrete on the properties of high performance recycled aggregate concrete [J]. *Construction and Building Materials*, 2015, **77**: 501 - 508. DOI:10.1016/j.conbuildmat.2014.12.035.
[7] Gonzalez-Corominas A, Etxeberria M. Effects of using recycled concrete aggregates on the shrinkage of high performance concrete [J]. *Construction and Building Materials*, 2016, **115**: 32 - 41. DOI:10.1016/j.conbuildmat.2016.04.031.
[8] Tabsh S W, Abdelfatah A S. Influence of recycled concrete aggregates on strength properties of concrete [J]. *Construction and Building Materials*, 2009, **23**(2): 1163 - 1167. DOI:10.1016/j.conbuildmat.2008.06.007.
[9] Xiao J Z, Li W G, Fan Y H, et al. An overview of study on recycled aggregate concrete in China (1996—2011) [J]. *Construction and Building Materials*, 2012, **31**: 364 - 383. DOI:10.1016/j.conbuildmat.2011.12.074.
[10] Kou S C, Poon C S, Etxeberria M. Influence of recycled aggregates on long term mechanical properties and pore size distribution of concrete [J]. *Cement and Concrete Composites*, 2011, **33**(2): 286 - 291. DOI:10.1016/j.cemconcomp.2010.10.003.
[11] Rahal K. Mechanical properties of concrete with recycled coarse aggregate [J]. *Building and Environment*, 2007, **42**(1): 407 - 415. DOI:10.1016/j.buildenv.2005.07.033.
[12] Koenders E A B, Pepe M, Martinelli E. Compressive strength and hydration processes of concrete with recycled aggregates [J]. *Cement and Concrete Research*, 2014, **56**: 203 - 212. DOI:10.1016/j.cemconres.2013.11.012.
[13] Li J B, Xiao J Z, Huang J. Influence of recycled coarse aggregate replacement percentages on compressive strength of concrete [J]. *Journal of Building Materials*, 2006, **9**(3): 297 - 301. DOI: 10.3969/j.issn.1007-9629.2006.03.008. (in Chinese)
[14] Kwan W H, Ramli M, Kam K J, et al. Influence of the amount of recycled coarse aggregate in concrete design and durability properties [J]. *Construction and Building Materials*, 2012, **26**(1): 565 - 573. DOI: 10.1016/j.conbuildmat.2011.06.059.
[15] Thomas C, Setién J, Polanco J A, et al. Durability of recycled aggregate concrete [J]. *Construction and Building Materials*, 2013, **40**: 1054 - 1065. DOI:10.1016/j.conbuildmat.2012.11.106.
[16] Levy S M, Helene P. Durability of recycled aggregates concrete: a safe way to sustainable development [J]. *Cement and Concrete Research*, 2004, **34**(11): 1975 - 1980. DOI:10.1016/j.cemconres.2004.02.009.
[17] Zega C J, Coelho dos Santos G S, Villagrán-Zaccardi Y A, et al. Performance of recycled concretes exposed to sulphate soil for 10 years [J]. *Construction and Building Materials*, 2016, **102**: 714 - 721. DOI:10.1016/j.conbuildmat.2015.11.025.
[18] Qi B, Gao J M, Chen F, et al. Evaluation of the damage process of recycled aggregate concrete under sulfate attack and wetting-drying cycles [J]. *Construction and Building Materials*, 2017, **138**: 254 - 262. DOI:10.1016/j.conbuildmat.2017.02.022.
[19] Gao J M, Yu Z X, Song L G, et al. Durability of concrete exposed to sulfate attack under flexural loading and drying-wetting cycles [J]. *Construction and Building Materials*, 2013, **39**: 33 - 38. DOI: 10.1016/j.conbuildmat.2012.05.033.
[20] Gao R D, Li Q B, Zhao S B. Concrete deterioration mechanisms under combined sulfate attack and flexural loading [J]. *Journal of Materials in Civil Engineering*, 2013, **25**(1): 39 - 44. DOI:10.1061/(asce)mt.1943-5533.0000538.
[21] Tsui N, Flatt R J, Scherer G W. Crystallization damage by sodium sulfate [J]. *Journal of Cultural Heritage*, 2003, **4**(2): 109 - 115. DOI:10.1016/s1296-2074(03)00022-0.

弯曲荷载对再生混凝土在硫酸盐侵蚀和干湿循环下劣化进程的影响

赵亚松　高建明　祁　兵　刘川北

(东南大学材料科学与工程学院, 南京 211189)
(东南大学江苏省土木工程材料重点实验室, 南京 211189)

摘要:研究了在干湿循环和弯曲荷载作用下再生混凝土硫酸盐侵蚀劣化进程. 试验中使用了 3 种不同的荷载率(0,0.3 和 0.5),通过对再生混凝土的相对动弹性模量和水溶性 SO_4^{2-} 含量的变化来研究其劣化进程. 并利用 XRD,ESEM 和 X-CT 等测试手段来研究再生混凝土劣化过程中内部产物与微结构的变化. 结果表明,弯曲荷载能够加速再生混凝土在硫酸盐侵蚀和干湿循环下的劣化,并且加快 SO_4^{2-} 向混凝土内部的传输速度. 这是因为随着荷载率的增加,再生混凝土的微裂纹会加速扩展,为 SO_4^{2-} 的传输提供更多的通道. 而 SO_4^{2-} 将会与水化产物反应生成膨胀性产物(石膏和钙矾石),进一步加速了再生混凝土的劣化过程.

关键词:再生混凝土;劣化;弯曲荷载;硫酸盐侵蚀;干湿循环
中图分类号:TU528